Article

Aminoxyl Radicals on the Silicon (001) Surface

Jennifer M. Bennett, Oliver Warschkow, and Nigel A. Marks

J. Phys. Chem. C, **2009**, 113 (3), 1020-1027 • Publication Date (Web): 23 December 2008

Aminoxyl Radicals on the Silicon (001) Surface

Jennifer M. Bennett,* Oliver Warschkow, and Nigel A. Marks

Centre for Quantum Computer Technology, School of Physics, The University of Sydney, Sydney, NSW, 2006, Australia

Received: August 13, 2008

Aminoxyl radicals form a class of persistent radical species of which the TEMPO (2,2,6,6-tetramethyl-1-piperidinyloxy) molecule is perhaps the best known. They are known to be dangling bond scavengers and bind readily to the silicon (001) surface. However, the possibility of the aminoxyl group reacting dissociatively with the surface has been largely ignored. Density functional theory is used to investigate possible reaction pathways for the simplest aminoxyl radical, H_2NO, on silicon. We consider same-site, same-dimer, and adjacent-dimer dissociation pathways and find that H_2NO dissociates readily in the presence of neighboring free dimers or dangling bonds. Further calculations examine the applicability of these findings to the larger dimethyl aminoxyl and TEMPO molecules.

1. Introduction

The ability to controllably modify the silicon surface with a large variety of organic molecules is an important skill in the development of molecular electronics.[1,2] Aminoxyl radicals (Figure 1) such as TEMPO (2,2,6,6-tetramethyl-1-piperidinyloxy) are one class of molecules that have been investigated in this context.[3−5] Characterized by a single unpaired electron on the oxygen atom, these molecules bind readily to exposed dangling bonds on the silicon surface by forming oxygen−silicon bonds.[6] The TEMPO radical also selectively binds to the single dangling bond of "missing hydrogen defects" on the hydrogen-terminated silicon surface.[7,8] These defects occur naturally owing to incomplete passivation of the surface with hydrogen. They can also be created deliberately using scanning tunneling microscopy (STM) H-lithography.[9−11] In the first case, the dangling bond scavenger nature of aminoxyl radicals can be used to create a surface free of reactive sites.[7,8] In the second case, hydrogen lithography makes it possible to accurately position molecules on the surface. Either way, once bound to the silicon surface, aminoxyl radicals are plausibly argued (e.g., ref 3, 6−8, 12) to be stable and not react further with the surface. However, it is not unreasonable to expect dissociation of the reactive oxygen−nitrogen bond, as this creates an amino fragment and an oxygen atom, both of which bind stably to the silicon surface. For example, breaking of the N−O bond is seen in the reaction of TEMPO with polyhydrosilanes, leading to the formation of a siloxane and an amine.[13] The reaction of organic nitro-compounds ($R-NO_2$) with the silicon surface also results in the breaking of N−O bonds and the subsequent insertion of oxygen into the surface.[14,15]

In this study, we use density functional theory (DFT) to investigate possible onward reactions of aminoxyl radicals bound to the silicon (001) surface. This reveals the conditions under which the aminoxyl N−O bond breaks and how the subsequent fragments react with the surface. The focus is primarily on the reaction pathways of the simplest aminoxyl radical, H_2NO, which serves here as a model system for larger aminoxyl radicals such as TEMPO. Although H_2NO itself is not a persistent radical in the laboratory, the small size of the molecule allows us to explore numerous reaction pathways of the aminoxyl functional group, that is, the N−O bond. We study the dissociation of the aminoxyl-group's N−O bond on three representative surface environments: a hydrogen-terminated surface with a single missing hydrogen defect, a clean surface with a single hydrogen forming an Si−Si−H hemihydride, and the clean surface with no hydrogen-termination. We find that with the increasing availability of reactive dangling bonds the dissociation of H_2NO becomes more likely. Further calculations using dimethyl aminoxyl, $(CH_3)_2NO$, confirm the relevance of our results to larger aminoxyl radicals. Finally, we consider the energetic stability of adsorbed and dissociated TEMPO radicals on the clean surface.

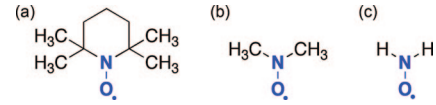

Figure 1. The chemical structures of (a) the TEMPO radical, (b) the dimethyl aminoxyl radical, $(CH_3)_2NO$, and (c) the simplest aminoxyl radical, H_2NO.

2. Computational Methodology

Calculations of structures, transition states, and energies are performed with the Gaussian 03 software.[16] Using a three-dimer $Si_{21}H_{20}$ cluster representation of the silicon (001) surface, formation energies are calculated using a compound model approach for the silicon surface.[17] This approach provides an economic approximation of energies at a higher target level of theory (here B3LYP functional, large basis set, and a three dimer $Si_{21}H_{20}$ cluster) by combining the results of several calculations conducted at a lower level. The approach we adopt here is to optimize the geometry of a structure at the low level of theory (PW91, small basis set) and then correct the calculated energy to account for the effect of using a more accurate level of theory (B3LYP) and a large basis set. The corrections are calculated from single-point energy calculations using either the improved level of theory or the larger basis set.

Two different composite basis sets are used in our calculations. The first composite basis set (labeled BS1) consists of

* Corresponding author. E-mail: jbell@physics.usyd.edu.au. Tel.: +61 2 9036 9085. Fax: +61 2 9351 7726.

10.1021/jp8065772 CCC: $40.75
Published on Web 12/23/2008

TABLE 1: Comparison of the Compound Model and the Target Level of Theory for a Set of Test Structures[a]

test structure[b]	$E_{clus} + E_{XCC}$ (eV)	E(B3LYP/BS1) (eV)	ΔE (eV)	$E_{clus} + E_{XCC} + E_{BSC}$ (eV)	E(B3LYP/BS2) (eV)	ΔE (eV)
A	− 2.60	− 2.61	0.01	− 2.64	− 2.68	0.04
D1	− 6.41	− 6.41	0.01	− 6.56	− 6.64	0.08
E1	− 5.82	− 5.83	0.01	− 6.01	− 6.08	0.08
TS(A → D1)[c]	− 1.09	− 1.09	0.00	− 1.16	− 1.23	0.06
TS(A → E1)	− 0.98	− 0.97	− 0.01	− 1.08	− 1.12	0.05

[a] The components of the compound model (E_{clus}, E_{XCC}, and E_{BSC}) are defined in the text. The composite basis sets, BS1 and BS2, are also defined in the text. [b] See Figure 2. [c] Transition state (TS)

the 6-311++G(d,p) basis set for the atoms of the top layer of the silicon surface and the molecular adsorbate, 6-311G(d,p) for the second layer of silicon atoms, and the LANL2DZ pseudopotential basis set for all other atoms. The second composite basis set (labeled BS2) is larger and consists of the 6-311++G(2df,2pd) basis set for the top layer of silicon and the molecule and 6-311G(2df,2pd) for all other atoms.

Our compound model calculations start with a structure optimization using the PW91 gradient-corrected density functional[18,19] together with the BS1 basis set. In the optimization, the cluster-terminating hydrogen atoms are held fixed[20] and all other atoms are free to relax. Using conventional quantum chemical notation, the initial cluster energy is given by the expression

$$E_{clus} = E(\text{PW91/BS1//PW91/BS1}) \quad (1)$$

This energy is combined with three correction terms (E_{ZPC}, E_{XCC}, E_{BSC}) accounting for vibrational zero point, exchange-correlation effects, and basis-set size. The vibrational-zero-point correction (E_{ZPC}) for a given structure is determined via a frequency calculation which also serves to characterize the structure as a local minimum or a transition state. The exchange-correlation correction (E_{XCC}) requires an additional single point energy calculation using the B3LYP functional[21,22] and the BS1 basis set. The correction term is the difference of the B3LYP and PW91 energies, that is,

$$E_{XCC} = E(\text{B3LYP/BS1//PW91/BS1}) - E(\text{PW91/BS1//PW91/BS1}) \quad (2)$$

The effect of this correction term is to switch the DFT functional from PW91 to the more accurate hybrid exact-exchange B3LYP functional. To understand this term, it is helpful to consider that the PW91 energy terms cancel when eq 1 and eq 2 are combined. Thus, the sum $E_{clus} + E_{XCC}$ is simply the B3LYP energy evaluated at the PW91 geometry.

The basis set correction E_{BSC} works in a similar way. We evaluate this correction using a single-point calculation of the PW91 energy using the larger BS2 basis set and subtract from it the PW91/BS1 energy. In quantum chemical notation this reads as follows:

$$E_{BSC} = E(\text{PW91/BS2//PW91/BS1}) - E(\text{PW91/BS1//PW91/BS1}) \quad (3)$$

Our compound model energy E is given by the combination of above terms

$$E = E_{clus} + E_{XCC} + E_{ZPC} + E_{BSC} \quad (4)$$

Throughout this paper, we report all energies and corrections as formation energies relative to the separated molecule and the cluster representing the relevant surface of interest (hydrogenated, hemihydride, or clean surface). Many of the structures have multiple buckling configurations of the bare Si−Si dimers, and for such cases we report only the lowest energy configuration.

To illustrate the performance of the compound model for the system studied, we have calculated formation energies for five selected structures directly at the B3LYP/BS1//B3LYP/BS1 and B3LYP/BS2//B3LYP/BS2 level of theory, that is, the target levels of theory that we seek to approximate. These structures are three minima (labeled A, D1, and E1) and two transition states [labeled TS(A → D1) and TS(A → E1)] taken from one of the reaction systems to be discussed in the Results section. In Table 1 we compare these energies with appropriate terms from the compound model. The first three columns of Table 1 compare the combination $E_{clus} + E_{XCC}$ with the directly computed B3LYP/BS1 energy of the B3LYP optimized structure. The difference between the models is less than 0.02 eV which shows that there is little benefit of conducting the optimization at the more expensive B3LYP level. The last three columns of Table 1 show how the combination of the compound model terms E_{clus}, E_{XCC}, and E_{BSC} compares to the directly calculated B3LYP/BS2//B3LYP/BS2 energies. Here the differences are somewhat larger, but generally less than 0.1 eV for all structures considered, which is an acceptable level of error for the purpose of this study. The advantage of the compound model is that it is considerably less expensive than the full B3LYP/BS2//B3LYP/BS2 level while still capturing much of its accuracy.

Transition states linking the minimum energy structures are computed using the quadratic synchronous transit (QST3)[23,24] method implemented in Gaussian 03.[16] This provides activation energies (E_A) allowing us to determine which reaction pathways are likely to occur. The temperatures of activation are calculated using the Arrhenius equation. For a given reaction time scale (or inverse rate) τ, the activation temperature T is given by

$$T = \frac{E_A}{k_B \ln(\tau A)} \quad (5)$$

where k_B is Boltzmann's constant. We will generally be interested in timescales relevant to STM experiments which typically range from minutes to hours. The attempt frequency, A, is estimated within harmonic transition state theory[25] using the expression

$$A = \prod_i \nu_i^{TS} / \prod_j \nu_j^{P} \quad (6)$$

where ν_i^{TS} and ν_j^{P} are the vibrational frequencies of the transition state and precursor structure, respectively. For example, in the reaction C1 → D4 (discussed in section 3.3 and shown in Figure 4), the vibrational frequencies of the transition state, TS(C1 → D4), and the minimum energy structure prior to reaction would be used to evaluate the attempt frequency A.

Exploratory calculations of the binding of TEMPO to the Si(001) surface are conducted using planewave/pseudopotential DFT as implemented in the VASP software.[26−29] These calculations use a three-dimensionally periodic model in which the silicon surface is represented by a slab of six atomic layers

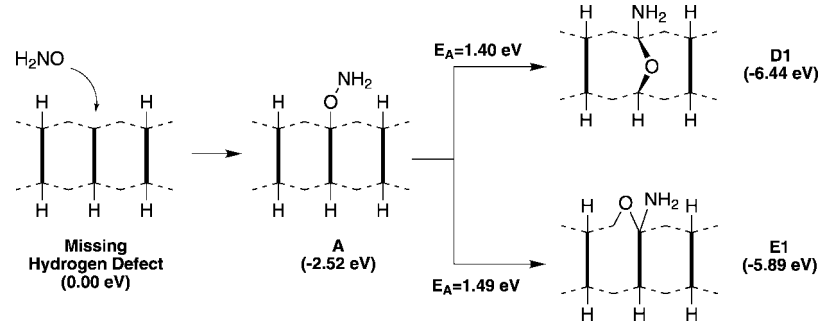

Figure 2. Reaction pathways of H_2NO binding to a missing hydrogen defect on the hydrogen-terminated silicon (001) surface. Formation energies of structures relative to the surface and molecule are given in brackets. The energies of activation, E_A, are given for each reaction.

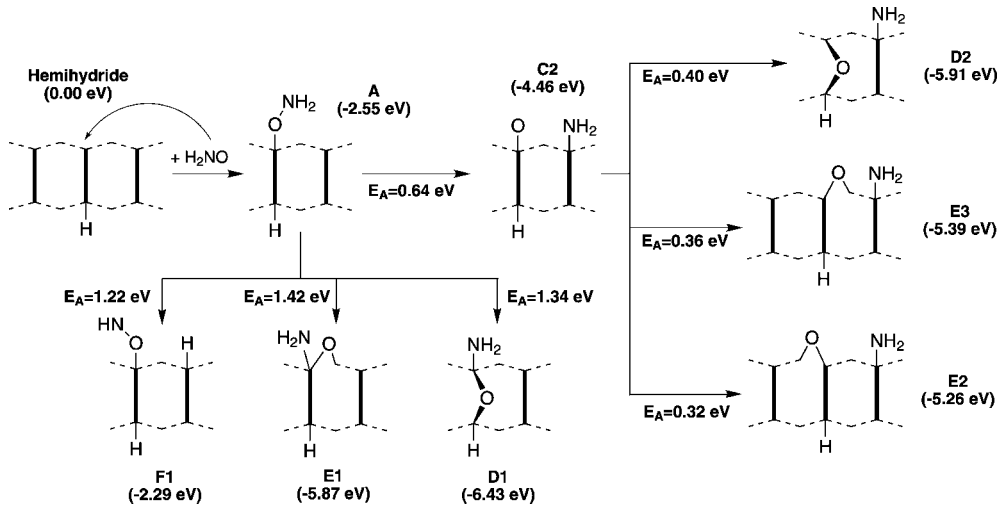

Figure 3. Reaction pathways of H_2NO binding to the free end of a hemihydride on the otherwise clean silicon (001) surface. Formation energies relative to the surface and molecule are given in brackets. The energies of activation E_A are given for each reaction step.

within a c(4 × 4) surface unit cell (i.e., four Si−Si dimers per primitive surface unit cell). TEMPO molecules are attached to the top surface of the slab at a density of one molecule per unit cell. Silicon atoms on the bottom surface of the slab are held fixed at bulk positions and their surface dangling bonds are saturated by hydrogen atoms in a quasi-dihydride termination [see ref 17 for details]. In the surface perpendicular direction, successive slabs are separated by approximately 11 Å of vacuum (from surface to surface). The vertical separation between an adsorbed TEMPO molecule and the next slab is at least 8 Å. In the horizontal direction, the TEMPO molecule is separated by at least 5 Å from its nearest periodic image. The DFT equations are solved in the generalized gradient approximation (PW91 functional)[19,18] using Vanderbilt ultrasoft pseudopotentials,[30,31] a planewave cutoff of 300 eV, and 4 × 4 × 1 Monkhorst-Pack[32] sampling of the irreducible Brillouin zone. Dipole corrections[33] are not applied in our calculations. Tests have confirmed that formation energies are not significantly affected (by less than 0.03 eV) when dipole corrections are included. Because of the cancelation of errors, the reaction energy that we report for the dissociation of the TEMPO molecule is even less sensitive to the dipole correction with changes significantly below 0.01 eV.

3. Results

For the purpose of this discussion it is convenient to categorize structures into five basic types. Type A has the H_2NO molecule bound via the oxygen atom to one end of a Si−Si dimer, while type B has the intact molecule forming two covalent bonds with the surface. In type C structures the molecule has dissociated into an oxygen adatom and an NH_2 fragment. Type D and E structures have the oxygen inserted into the Si−Si dimer and backbond, respectively. Type F structures result from a dissociation of the N−H bond in the aminoxyl molecule. Transition state structures are labeled according to the minima they connect, with the precursor structure listed first. Labeling structures in this manner facilitates the comparison of analogous structures on the clean and hydrogenated surfaces. We also distinguish between three prototype reactions of H_2NO dissociation: single-site, single-dimer, and adjacent-dimer. These involve a single Si atom, two Si atoms on the same dimer, and two Si atoms on adjacent dimers, respectively.

3.1. H_2NO Reaction with a Missing Hydrogen Defect. Hydrogen termination of the Si(001) surface dramatically reduces its chemical reactivity due to the saturation of the dangling bonds. When one of these hydrogen atoms is missing, the exposed dangling bond forms a local and highly reactive site. As described in Figure 2 and Table 2, H_2NO reacts with the dangling bond in a barrierless reaction, binding to the surface via an Si−O bond (structure A), with an energy gain of 2.52 eV. As the surrounding sites are unreactive, the most plausible dissociation reactions are single-site, that is, centered on the silicon atom to which the molecule is bound. We consider two single-site pathways in which the molecule breaks apart, producing separated oxygen and NH_2. The NH_2 fragment binds directly to the Si atom and the oxygen atom inserts into either the Si−Si dimer (leading to structure D1) or the Si−Si backbond (forming structure E1). These oxygen-inserted structures D1 and E1 are considerably more stable than the initial structure A, with respective energy gains of 3.93 and 3.38 eV. However,

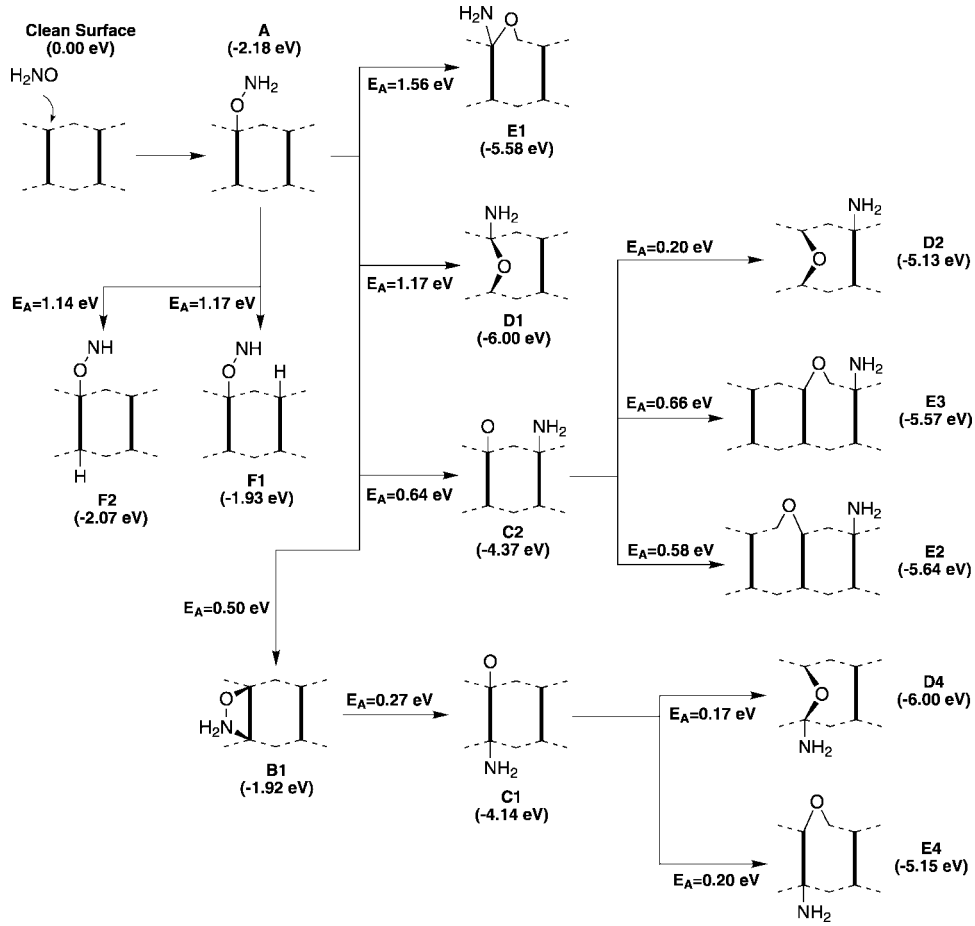

Figure 4. Reaction pathways of H_2NO binding and dissociating on the clean silicon (001) surface. Formation energies relative to the surface and molecule are given in brackets. The activation energies, E_A, are given for each step.

TABLE 2: Calculated Formation Energies (E) of Intermediates and Transition States of the Possible Reaction Pathways of H_2NO with a Missing Hydrogen Defect. Also Given Are the Four Energy Terms (E_{clus}, E_{XCC}, E_{ZPC} and E_{BSC}) of the Compound Model, which Contribute to the Formation Energy

		energy terms (eV)			
structure[a]	E (eV)	E_{clus}	E_{XCC}	E_{ZPC}	E_{BSC}
A	− 2.52	− 2.63	0.03	0.13	− 0.04
TS(A → D1)[b]	− 1.11	− 1.51	0.42	0.05	− 0.07
D1	− 6.44	− 6.09	− 0.31	0.12	− 0.16
TS(A → E1)	− 1.03	− 1.44	0.46	0.05	− 0.10
E1	− 5.89	− 5.59	− 0.23	0.12	− 0.19

[a] See Figure 2. [b] Transition state (TS).

TABLE 3: Activation Energies (E_A), Reaction Energies (ΔE), Attempt Frequencies (A) and Temperatures of Activation for the Reaction of H_2NO with a Missing Hydrogen Defect

				temperature[b] (K)		
reaction[a]	E_A (eV)	ΔE (eV)	A (THz)	1 s	1 min	1 h
A → D1	1.40	− 3.93	13.4	538	473	423
A → E1	1.49	− 3.38	12.8	573	505	451

[a] See Figure 2. [b] Temperatures of activation are given for three representative reaction timescales (τ).

the calculated activation energies of 1.40 eV (D1) and 1.49 eV (E1) are significantly larger than the ≈ 1 eV activation energy typically available at room temperature (assuming STM timescales of minutes to hours). This indicates that the aminoxyl molecule will not dissociate at this temperature. From the calculated activation temperatures for these reactions (Table 3) we expect that H_2NO dissociation and surface oxidation will commence at ≈ 450 K. In this context we note the importance of the compound model used in this work. If one considers a prototypical gradient-corrected DFT calculation, amounting to neglect of the exact-exchange-based E_{XCC} term, then the activation barriers for dissociation to D1 and E1 reduce to 1.01 and 1.05 eV, respectively. At this level of theory an appreciable rate of dissociation would be predicted at room temperature.

3.2. H_2NO Reaction with a Hemihydride on a Clean Surface. In the reactions of H_2NO with the missing hydrogen defect (see previous section) the possibilities for dissociation were limited by the passivation of the neighboring dimers. To explore the effect that adjacent dangling bonds have on the dissociation pathway, we now consider the same molecule bound to the dangling bond of a hemihydride on the clean surface (Figure 3 and Table 4). Unsurprisingly, the single-site reaction pathways A → D1 and A → E1 for the hemihydride system (Figure 3) have reaction energies and activation barriers very similar to those seen for the missing hydrogen defect (Figure 2). However, the presence of reactive free silicon dimers adjacent to the hemihydride makes adjacent-dimer reactions possible. In particular, the molecular adsorbate can use a neighboring dimer to dissociate into oxygen and NH_2. During the transition the molecule leans across to the adjacent dimer. A new bond between the nitrogen and silicon is formed and the N−O bond is broken. The resulting structure, C2, is 1.91

TABLE 4: Calculated Formation Energies of Intermediates and Transition States for the Reaction Pathways of H_2NO with the Clean Surface Containing a Hemihydride. Also Given Are the Four Energy Terms of the Compound Model Which Contribute to the Formation Energ.

		energy terms (eV)			
structure[a]	E (eV)	E_{clus}	E_{XCC}	E_{ZPC}	E_{BSC}
A	− 2.55	− 2.66	0.02	0.13	− 0.05
TS(A → D1)	− 1.21	− 1.62	0.40	0.06	− 0.04
D1	− 6.43	− 6.11	− 0.32	0.12	− 0.13
TS(A → E1)	− 1.13	− 1.55	0.46	0.05	− 0.09
E1	− 5.87	− 5.61	− 0.21	0.11	− 0.15
TS(A → F1)	− 1.32	− 1.48	0.13	− 0.07	0.09
F1	− 2.29	− 2.14	− 0.22	− 0.01	0.09
TS(A → C2)	− 1.91	− 2.45	0.38	0.09	0.07
C2	− 4.46	− 4.47	0.02	0.09	− 0.11
TS(C2 → D2)	− 4.06	− 3.97	− 0.06	0.07	− 0.10
D2	− 5.91	− 5.54	− 0.43	0.12	− 0.06
TS(C2 → E2)	− 4.14	− 4.13	− 0.04	0.08	− 0.04
E2	− 5.26	− 5.02	− 0.34	0.10	0.00
TS(C2 → E3)	− 4.10	− 4.04	− 0.07	0.06	− 0.06
E3	− 5.39	− 5.06	− 0.36	0.11	− 0.08

[a] See Figure 3.

TABLE 5: Activation Energies (E_A), Reaction Energies (ΔE), Attempt Frequencies (A) and Temperatures of Activation for the Reaction of H_2NO with a Hemihydride on an Otherwise Clean Silicon (001) Surface

				temperature[b] (K)		
reaction[a]	E_A (eV)	ΔE (eV)	A (THz)	1 s	1 min	1 h
A → D1	1.34	− 3.89	7.0	526	462	412
A → E1	1.42	− 3.32	10.5	550	484	432
A → F1	1.22	+ 0.26	4.3	526	462	412
A → C2	0.64	− 1.92	1.4	266	232	205
C2 → D2	0.40	− 1.45	6.7	157	138	123
C2 → E2	0.32	− 0.79	3.9	128	112	100
C2 → E3	0.36	− 0.93	15.1	138	121	108

[a] See Figure 3. [b] Temperatures of activation are given for three representative reaction timescales (τ).

eV more stable than A and contains an isolated oxygen adatom and a NH_2 fragment bound to different dimers. Although C2 is more than 1.5 eV less stable than either D1 or E1, the activation energy to form C2 is considerably lower. Moreover, oxygen adatoms are well-known to insert into Si−Si dimer or backbonds with little activation.[34−36] Accordingly, structure C2 stabilizes with 0.32−0.40 eV activation to form three kinds of oxygen inserted structures. These three structures have the oxygen inserted into either the dimer bond (D2) or one of the two backbonds of the hemihydride (E2 and E3), with the NH_2 fragment always bound to the adjacent dimer.

The possibility of the aminoxyl adsorbate (structure A) dissociating via a breaking of an N−H bond instead of an N−O bond is also investigated. The dissociation produces structure F1, in which the two resulting fragments H and HNO are bound to adjacent dimers. The calculated activation barrier for the reaction is 1.22 eV. Therefore, the dissociation of structure A by hydrogen shift is not competitive with the N−O bond breaking process (A to C2) which is activated at 0.64 eV.

Looking now at the calculated temperatures of activation (Table 5), we can discuss the conditions under which these reactions are likely to occur. The same-site reactions (A → D1 and A → E1) have very similar activation barriers to those on the hydrogenated surface and are therefore activated at similar temperatures. These reactions, however, cannot compete with adjacent-dimer dissociation which becomes activated around 230 K. The first reaction step, A → C2, is rate-determining with the onward reactions (C2 → D2, C2 → E2, and C2 → E3) activated at even lower temperature. The similarity of the activation temperatures indicates that all three oxygen-inserted structures will form.

TABLE 6: Calculated Formation Energies of Intermediates and Transition States of the Reaction Pathways of H_2NO with the Clean Silicon (001) Surface. Also Given Are the Four Energy Terms of the Compound Model Contributing to the Formation Energy

		energy terms (eV)			
structure[a]	E (eV)	E_{clus}	E_{XCC}	E_{ZPC}	E_{BSC}
A	− 2.18	− 2.26	− 0.07	0.14	0.02
TS(A → D1)	− 1.00	− 1.37	0.30	0.07	0.00
D1	− 6.00	− 5.65	− 0.41	0.12	− 0.06
TS(A → E1)	− 0.62	− 1.08	0.39	0.05	0.01
E1	− 5.58	− 5.27	− 0.31	0.12	− 0.11
TS(A → F1)	− 1.01	− 1.11	0.01	− 0.05	0.14
F1	− 1.93	− 1.74	− 0.34	0.00	0.15
TS(A → F2)	− 1.04	− 1.24	0.16	− 0.05	0.09
F2	− 2.07	− 1.93	− 0.21	0.00	0.07
TS(A → B1)	− 1.68	− 2.05	0.20	0.14	0.04
B1	− 1.92	− 2.38	0.19	0.17	0.10
TS(B1 → C1)	− 1.65	− 2.14	0.33	0.11	0.05
C1	− 4.14	− 4.18	− 0.07	0.08	0.02
TS(C1 → D4)	− 3.97	− 3.94	− 0.04	0.09	− 0.09
D4	− 6.00	− 5.65	− 0.41	0.12	− 0.06
TS(C1 → E4)	− 3.94	− 3.87	− 0.05	0.07	− 0.09
E4	− 5.15	− 4.81	− 0.35	0.11	− 0.10
TS(A → C2)	− 1.54	− 2.01	0.24	0.10	0.13
C2	− 4.37	− 4.45	− 0.17	0.11	0.14
TS(C2 → D2)	− 4.17	− 4.15	− 0.11	0.10	− 0.01
D2	− 5.13	− 4.95	− 0.34	0.09	0.08
TS(C2 → E2)	− 3.80	− 3.69	− 0.16	0.07	− 0.02
E2	− 5.64	− 5.30	− 0.32	0.11	− 0.13
TS(C2 → E3)	− 3.72	− 3.86	0.01	0.09	0.04
E3	− 5.57	− 5.27	− 0.33	0.12	− 0.10

[a] See Figure 4.

3.3. H_2NO Reaction with the Clean Surface. We now consider the adsorption and dissociation of H_2NO on a completely free silicon (001) surface. The absence of the hemihydride hydrogen atom brings the other end of the dimer into play, leading to an even larger variety of possible reactions (Figure 4 and Table 6). In addition to same-site dissociation (e.g., A → D1) and adjacent-dimer dissociation (A → C2), the H_2NO radical on the clean surface can dissociate across a single dimer in a same-dimer reaction (A → B1 → C1). The new set of reactions begin with the adsorbate molecule forming a four-membered ring structure (B1) with the dimer. Although B1 has a higher energy than the precursor structure A, the onward reaction has a low barrier (0.26 eV) and leads to an overall energy gain of 1.96 eV. This produces structure C1 which consists of an NH_2 fragment and an oxygen atom attached to opposite ends of the same dimer. Structure C1 can further stabilize by inserting the oxygen atom into the dimer bond (structure D4) or one of the two backbonds (structure E4) with barriers of less than 0.21 eV. We note that D1 and D4 have the same structure but different orientations due to the different pathways leading to their formation. Interestingly, it is the more complicated four-step pathway that has the lower overall reaction barrier (0.52 eV for A → D4 versus 1.18 eV for A → D1). Dissociation of the aminoxyl molecular adsorbate (structure A) by N−H bond breaking leads to structures F1 and F2, in which the HNO and H fragments are bonded to adjacent and same dimers, respectively. As was found for the hemihydride

TABLE 7: Activation Energies (E_A), Reaction Energies (ΔE), Attempt Frequencies (A) and Temperatures of Activation for the Reaction of H_2NO with the Clean Silicon (001) Surface

				temperature[b] (K)		
reaction[a]	E_A (eV)	ΔE (eV)	A (THz)	1 s	1 min	1 h
A → D1	1.17	− 3.83	7.8	457	402	359
A → E1	1.56	− 3.41	17.4	594	524	468
A → F1	1.17	+ 0.25	3.0	473	414	368
A → F2	1.14	+ 0.11	5.0	452	397	353
A → C1	0.52	− 1.97	1.4	216	188	167
C1 → D4	0.17	− 1.86	1.1	71	62	55
C1 → E4	0.20	− 1.00	3.4	80	70	63
A → C2	0.64	− 2.20	2.8	259	227	202
C2 → D2	0.20	− 0.76	4.5	80	70	62
C2 → E2	0.58	− 1.26	18.8	220	194	174
C2 → E3	0.66	− 1.20	4.5	263	231	205

[a] See Figure 4. [b] Temperatures of activation are given for three representative reaction timescales (τ).

surface, the hydrogen shift barriers (1.17 and 1.14 eV) are higher and thus less favorable than the lowest N−O dissociation barriers (0.64 and 0.52 eV).

An important aspect of adsorption onto the clean surface is that the aminoxyl radical creates, rather than passivates, a surface dangling bond. The presence of this dangling bond has a noticeable effect on the oxygen-insertion reactions proceeding from structure C2. When a hemihydride is involved in the reaction, the energy barriers for the insertion of oxygen into a dimer bond or backbond are very similar (Table 4). In contrast, the barrier on the clean surface for incorporation into the dimer (forming D2) is more than 0.38 eV lower than the barriers for backbond incorporation (leading to E2 and E3). These differences extend to the relative stability of the oxygen-inserted structures, with D2 the most stable (by over 0.5 eV) on the hemihydride surface and the least stable (by over 0.4 eV) on the clean surface. In passing, we note that the aminoxyl radical affects the relative energetics between structures C1 and C2 in a nonintuitive way. For a closed-shell system one would expect single-dimer structures such as C1 to be preferred, but when an extra electron is present this is not necessarily the case.

To assess the relatively likelihood of the different reactions we once more compute the temperatures of activation (Table 7). Same-dimer (A → C1) and adjacent-dimer reactions (A → C2) proceed at similar temperatures (around 200 K) while same-site reactions require much higher temperatures. From structure C1 the oxygen will quickly insert into either a backbond (structure E4) or a dimer bond (structure D4), and as the activation temperatures are so similar, both are likely to occur. As discussed above, there is a distinct preference for structure C2 to insert the oxygen into the dimer bond, forming structure D2. In summary, the reaction pathways most likely to occur for H_2NO on clean silicon (001) are A → B1 → C1 → D4, A → B1 → C1 → E4, and A → C2 → D2.

3.4. Dimethyl Aminoxyl Radical on the Clean Surface. Having established the reactions for the H_2NO radical, we now consider the effect of alkyl substitutions on the NH_2 group, using dimethyl aminoxyl, $(CH_3)_2NO$, as an example. We take two of the preferred routes of the H_2NO reactions on the clean surface, A → B1 → C1 → D4 and A → C2 → D2, as illustrative examples and additionally consider an alternative dissociation route involving a hydrogen shift.

The pathways and formation energies of these reactions are shown in Figure 5. There is a close correspondence to the equivalent reaction pathways found for H_2NO, with formation energies, transition states, and geometries broadly similar. These similarities suggest that the reaction pathways calculated for the dissociation of H_2NO on the silicon (001) surface are qualitatively representative of larger aminoxyl radicals. A direct comparison of the activation energies for the dissociation of H_2NO and $(CH_3)_2NO$ is made in Table 8. This reveals the general trend that reactions involving the larger molecule have slightly higher activation energies, presumably due to steric effects.

TABLE 8: Comparison of Reaction Barriers for H_2NO and $(CH_3)_2NO$ on the Clean Silicon (001) Surfac.

	activation energy (eV)	
reaction[a]	H_2NO	$(CH_3)_2NO$
A → C1	0.52	0.64
C1 → D4	0.17	0.30
A → C2	0.64	0.66
C2 → D2	0.20	0.31

[a] See Figure 4 and Figure 5.

We have also tested whether the dimethyl aminoxyl adsorbate can dissociate via a shift of a proton from a methyl group to the surface. This reaction is considered because of its analogy with the α-carbon deprotonation reaction that is common for ketones.[37,38] For ketones (e.g., acetone) this reaction produces an enolate fragment and a hydrogen atom attached to the silicon surface. We find that the corresponding product for dimethyl aminoxyl (structure F3 in Figure 5) is not a potential energy minimum. The structure spontaneously relaxes to form a six-membered ring structure with the neighboring dimer (structure F4). The transition state corresponds to the hydrogen shift part of the reaction. The calculated activation barrier for this reaction is 1.01 eV which is considerably higher than either of the two N−O bond breaking reactions (0.64 and 0.66 eV).

3.5. TEMPO on the Clean Surface. The results of the previous sections suggest that dissociation of TEMPO on the clean surface should be considered as a possibility. In particular, we have shown that the aminoxyl functional group is prone to undergo N−O bond breaking with an appreciable rate at room temperature and is driven by a considerable thermodynamic energy gain. TEMPO, however, is designed such that the chemical reactivity of the aminoxyl group is sterically protected by the heavily methylated piperidinyl ring. This suppresses, among other reactions, dimerization between pairs of TEMPO molecules. This poses the question: Can these steric constraints also suppress TEMPO dissociation on the clean surface?

To address this question we compute the binding energy of TEMPO on the surface, before and after dissociation. This will show as whether dissociation is still an exothermic process or whether steric constraints render the reaction unfavorable. To adequately describe the steric energy penalty it is necessary to include a representation of the adjacent dimer row in the model. We do this by switching to a periodic slab model of the surface shown in Figure 6a. We use a c(4 × 4) unit cell which is sufficiently large to separate the TEMPO molecule from its periodic images.

Figures 6b and 6c show side views of adsorbed and dissociated TEMPO on the clean surface. In the adsorbed configuration (Figure 6b) the TEMPO molecule is standing upright, with the N−O bond acting as a "spacer" between the molecule and the surface. We considered two conformations of the adsorbed TEMPO molecule: the structure shown is the more stable of the two. The dissociated configuration in Figure

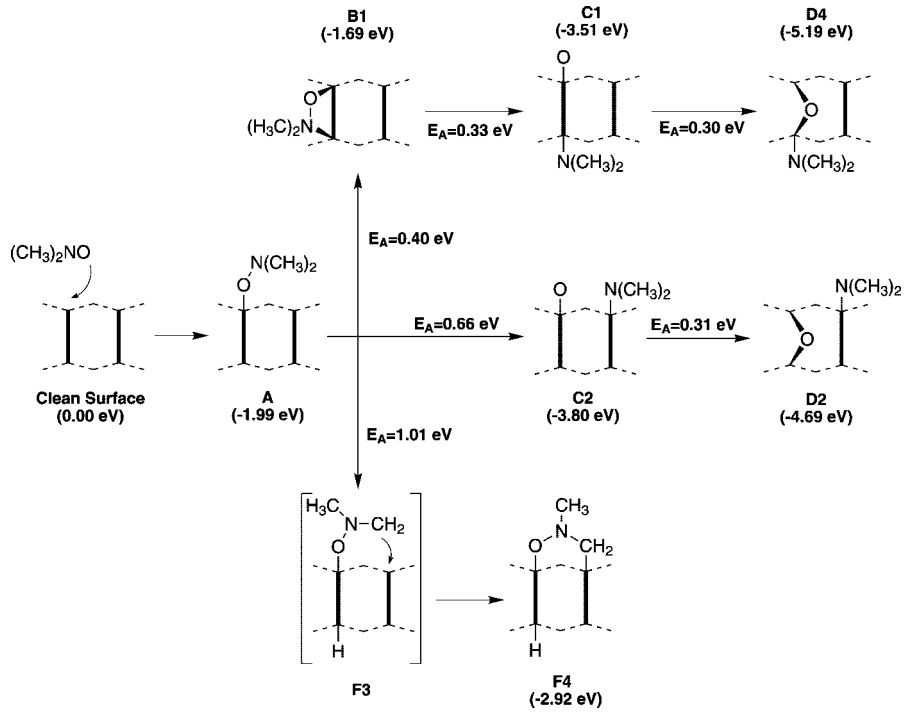

Figure 5. Two possible dissociation pathways for $(CH_3)_2NO$ on the clean silicon (001) surface. Formation energies relative to the clean surface and molecule are given in brackets. The energies of activation are shown for each transition.

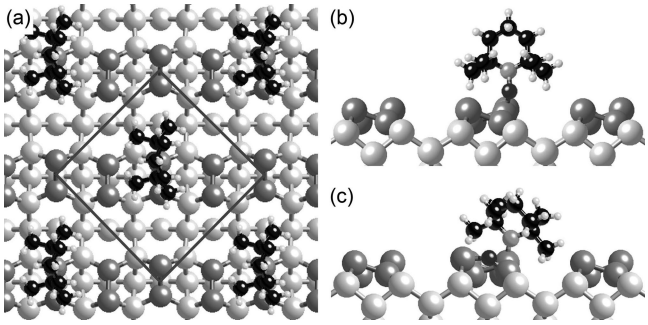

Figure 6. (a) Top view of the TEMPO molecule (Figure 1a) adsorbed on the silicon (001) surface. Solid lines indicate the c(4 × 4) cell used in the VASP calculations. (b) Side view of a single adsorbed TEMPO molecule on the surface (structure A). For clarity, the periodically repeated molecules are not shown. (c) Side view of the dissociated TEMPO molecule with the oxygen atom incorporated into the Si−Si dimer (structure D2).

6c is a D2-like structure in which the oxygen atom is inserted into the Si−Si dimer and the piperidinyl ring is directly attached to the surface. We find that this dissociated structure is 2.3 eV more stable than the adsorbed configuration. This energy gain is slightly less than the 2.7 eV gain for the equivalent reaction between dimethyl aminoxyl and the clean surface. Although different methods were used to compute these energy gains, it is likely that steric effects contribute to some of this difference. Figure 6c helps us to understand why the energy penalty from steric interactions is comparatively small: in the dissociated configuration the TEMPO fragment leans neatly into the valley between the dimer rows. Because of prohibitive computational cost we cannot compute the dissociation reaction barrier with either our VASP or Gaussian approaches. However, it is reasonable to speculate that TEMPO dissociation might indeed be possible on the clean surface.

4. Discussion and Conclusions

The principal result of this study is the finding that the N−O bond in aminoxyl radicals rapidly dissociates on the silicon surface at room temperature when dangling bonds are available nearby. Even when surrounding dangling bonds are passivated, dissociation is still possible provided elevated temperatures (450−500 K) are used. Although there is every reason to believe that these processes will occur (due to the higher relative stability of the Si−O bond), we are unaware of any experimental or theoretical investigations of these dissociation processes.

The main point of contact between this work and the literature concerns the N−O−Si bond found in structure A. Both H_2NO and $(CH_3)_2NO$ initially bind to the clean silicon surface via a Si−O bond with formation energies of − 2.18 and − 1.99 eV, respectively. This first step is in close agreement with DFT calculations by Greene et al.,[6] who find the binding energy of the TEMPO molecule on a cluster representation of the clean surface to be 1.9−2.0 eV. Our binding energy of TEMPO onto a periodic slab representation is slightly higher at 2.5 eV.

From a structural point-of-view, the combination of an undissociated aminoxyl and a hemihydride (structure A, Figure 3) closely resembles the proposed end-product of a reaction between hydroxylamines and the clean silicon surface.[39] Hydroxylamines are very similar to aminoxyl radicals, differing only by the extra hydrogen atom attached to the oxygen. As demonstrated by the study of diethylhydroxylamine (DEHA), $(C_2H_5)_2NOH$, by DiLabio et al.,[39] the reaction of hydroxylamines with the clean surface results in an aminoxyl molecule bound to the surface by an O−Si bond and an H bonded to the other Si of the same dimer. Our calculations suggest that this structure could react further by dissociating the N−O bond and inserting oxygen into a Si−Si bond (cf. structures D2, E2, and E3 in Figure 3).

Another point of contact concerns the *absence* of room-temperature dissociation on the hydrogenated surface. In this instance, our studies of the missing hydrogen defect find significant barriers to the dissociation of aminoxyl radicals bound to the defect site. Our results are thus consistent with the STM experiments of Pitters et al.[7,8] who find that TEMPO molecules can be placed at missing hydrogen defect sites and removed

again. We therefore agree with their conclusion that TEMPO is stable on the hydrogen-terminated silicon surface. Given that we have shown that dissociation of TEMPO is exothermic, it would be interesting to consider whether adsorption and STM-induced desorption is possible on the clean surface. This would reveal whether TEMPO can dissociate in the manner of the smaller aminoxyl radicals or instead is kinetically stabilized by steric effects increasing the activation energy required for the reaction to proceed.

Acknowledgment. This work was supported by the Australian Research Council, the Australian Government, the U.S. Advanced Research and Development Activity, National Security Agency, and Army Research Office under Contract No. DAAD19-01-1-0653. Computing support was provided by the Australian Partnership for Advanced Computing (APAC).

References and Notes

(1) Wolkow, R. A. *Annu. Rev. Phys. Chem.* **1999**, *50*, 413.
(2) Filler, M. A.; Bent, S. F. *Prog. Surf. Sci.* **2003**, *73*, 1.
(3) Guisinger, N. P.; Greene, M. E.; Basu, R.; Baluch, A. S.; Hersam, M. C. *Nano Lett.* **2004**, *4* (1), 55.
(4) Guisinger, N. P.; Basu, R.; Greene, M. E.; Baluch, A. S.; Hersam, M. C. *Nanotechnology* **2004**, *15*, S452.
(5) Rakshit, T.; Liang, G.-C.; Ghosh, A. W.; Datta, S. *Nano Lett.* **2004**, *4* (10), 1803.
(6) Greene, M. E.; Guisinger, N. P.; Basu, R.; Baluch, A. S.; Hersam, M. C. *Surf. Sci.* **2004**, *559*, 16.
(7) Pitters, J. L.; Piva, P. G.; Tong, X.; Wolkow, R. A. *Nano Lett.* **2003**, *3* (10), 1431.
(8) Pitters, J. L.; Wolkow, R. A. *J. Am. Chem. Soc.* **2005**, *127*, 48.
(9) Lyding, J. W.; Shen, T.-C.; Hubacek, J. S.; Tucker, J. R.; Abeln, G. C. *Appl. Phys. Lett.* **1994**, *64*, 2010.
(10) Shen, T.-C.; Wang, C.; Abeln, G. C.; Tucker, J. R.; Lyding, J. W.; Avouris, P.; Walkup, R. W. *Science* **1995**, *268* (5217), 1590.
(11) Tucker, J. R.; Shen, T.-C *Int. J. Circ. Theor. Appl.* **2000**, *28*, 553.
(12) Basu, R.; Guisinger, N. P.; Greene, M. E.; Hersam, M. C. *App. Phys. Lett.* **2004**, *85* (13), 2619.
(13) Chatgilialogu, C.; Guerrini, A.; Lucarini, M.; Pedulli, G. F.; Carrozza, P.; Roit, G. D.; Borazatta, V.; Lucchini, V. *Organometallics* **1998**, *17*, 2169.
(14) Barriocanal, J. A.; Doren, D. J. *J. Phys. Chem. B* **2000**, *104*, 12269.
(15) Méndez De Leo, L. P.; Teplyakov, A. V *J. Phys. Chem. B* **2006**, *110*, 6899.
(16) Frisch, M. J.; Trucks, G. W.; Schlegel, H. B.; Scuseria, G. E.; Robb, M. A.; Cheeseman, J. R.; Montgomery, Jr., J. A.; Vreven, T.; Kudin, K. N.; Burant, J. C.; Millam, J. M.; Iyengar, S. S.; Tomasi, J.; Barone, V.; Mennucci, B.; Cossi, M.; Scalmani, G.; Rega, N.; Petersson, G. A.; Nakatsuji, H.; Hada, M.; Ehara, M.; Toyota, K.; Fukuda, R.; Hasegawa, J.; Ishida, M.; Nakajima, T.; Honda, Y.; Kitao, O.; Nakai, H.; Klene, M.; Li, X.; Knox, J. E.; Hratchian, H. P.; Cross, J. B.; Bakken, V.; Adamo, C.; Jaramillo, J.; Gomperts, R.; Stratmann, R. E.; Yazyev, O.; Austin, A. J.; Cammi, R.; Pomelli, C.; Ochterski, J. W.; Ayala, P. Y.; Morokuma, K.; Voth, G. A.; Salvador, P.; Dannenberg, J. J.; Zakrzewski, V. G.; Dapprich, S.; Daniels, A. D.; Strain, M. C.; Farkas, O.; Malick, D. K.; Rabuck, A. D.; Raghavachari, K.; Foresman, J. B.; Ortiz, J. V.; Cui, Q.; Baboul, A. G.; Clifford, S.; Cioslowski, J.; Stefanov, B. B.; Liu, G.; Liashenko, A.; Piskorz, P.; Komaromi, I.; Martin, R. L.; Fox, D. J.; Keith, T.; Al-Laham, M. A.; Peng, C. Y.; Nanayakkara, A.; Challacombe, M.; Gill, P. M. W.; Johnson, B.; Chen, W.; Wong, M. W.; Gonzalez, C.; Pople, J. A. *Gaussian 03*, revision D.01; Gaussian, Inc.: Wallingford, CT, 2004.
(17) Warschkow, O.; McDonell, T. L.; Marks, N. A. *Surf. Sci.* **2007**, *601*, 3020.
(18) Perdew, J. P.; Chevary, J. A.; Vosko, S. H.; Jackson, K. A.; Pederson, M. R.; Singh, D. J. *Phys. Rev. B* **1992**, *46* (11), 6671.
(19) Perdew, J. P.; Wang, Y. *Phys. Rev. B* **1992**, *45* (23), 13244.
(20) The positions of the cluster-terminating hydrogen atoms are the same in all our calculations. The procedure by which these positions were determined is described in ref 17.
(21) Becke, A. D. *Phys. Rev. A* **1988**, *38* (6), 3098–3100.
(22) Lee, C.; Yang, W.; Parr, R. G. *Phys. Rev. B* **1988**, *37* (2), 785.
(23) Peng, C.; Schlegel, H. B. *Isr. J. Chem.* **1993**, *33*, 449.
(24) Peng, C.; Ayala, P. Y.; Schlegel, H. B.; Frisch, M. J. *J. Comput. Chem.* **1996**, *17* (1), 49.
(25) Vineyard, G. H. *J. Phys. Chem. Solids* **1957**, *3*, 121.
(26) Kresse, G.; Hafner, J. *Phys. Rev. B* **1993**, *47*, 558.
(27) Kresse, G.; Hafner, J. *Phys. Rev. B* **1994**, *49*, 14251.
(28) Kresse, G.; Furthmüller, J. *Comput. Mater. Sci.* **1996**, *6*, 15.
(29) Kresse, G.; Furthmüller, J. *Phys. Rev. B* **1996**, *54*, 11169.
(30) Vanderbilt, D. *Phys. Rev. B* **1990**, *41*, 7892.
(31) Kresse, G.; Hafner, J. *J. Phys.: Condens. Matter* **1994**, *6*, 8245.
(32) Monkhorst, H. J.; Pack, J. D. *Phys. Rev. B* **1976**, *13*, 5188.
(33) Makov, G.; Payne, M. C. *Phys. Rev. B* **1995**, *51* (7), 4014.
(34) Kato, K.; Uda, T. *Phys. Rev. B* **2000**, *62* (23), 62.
(35) Hemeryck, A.; Mayne, A. J.; Richard, N.; Estève, A.; Chabal, Y. J.; Djafari Rouhani, M.; Dujardin, G.; Comtet, G. *J. Chem. Phys.* **2007**, *126*, 114707.
(36) Hemeryck, A.; Richard, N.; Estève, A.; Djafari Rouhani, M. *Surf. Sci.* **2007**, *601*, 2339.
(37) Wang, G. T.; Mui, C.; Musgrave, C. B.; Bent, S. F. *J. Phys. Chem. B* **2001**, *105*, 12559.
(38) Schofield, S. R.; Saraireh, S. A.; Smith, P. V.; Radny, M. W.; King, B. V. *J. Am. Chem. Soc.* **2007**, *129*, 11402.
(39) DiLabio, G. A.; Dogel, S. A.; Anagaw, A.; Pitters, J. L.; Wolkow, R. A. *Phys. Chem. Chem. Phys.* **2007**, *9*, 1629.

JP8065772